# Additional File 1

This Additional File 1 provides supplementary figures and tables that complement and extend the analyses presented in the main text. These materials include regional time series of malaria incidence, CwDMD fitting and decomposition results, and demographic and geographic attributes of the study areas. Specifically, Section 1 presents analyses at the scale of 17 administrative regions, while Section 2 focuses on a finer resolution of 37 subdivided regions. Together, these supplementary materials provide additional context for interpreting the spatiotemporal transmission dynamics identified in the main analyses and support the reproducibility of the study.

## Section 1. Analyses for 17 Administrative Regions

- Fig. S1 - Monthly malaria cases across 17 regions of South Korea (2001–2024)
- Tab. S1 - Demographic and malaria statistics across 17 administrative regions

## Section 2. Analyses for 37 Subdivided Regions

- Fig. S2 - Subdivision of 37 high-risk regions for CwDMD analysis
- Tab. S2 - Total malaria cases by region in 2007, 2011, 2018, and 2023
- Fig. S3 - Eigenvalue spectra of CwDMD analysis in 2007, 2011, 2018, and 2023
- Fig. S4 - Observed vs. reconstructed weekly malaria cases in 2007 (37 regions)
- Fig. S5 - Observed vs. reconstructed weekly malaria cases in 2011 (37 regions)
- Fig. S6 - Observed vs. reconstructed weekly malaria cases in 2018 (37 regions)
- Fig. S7 - Observed vs. reconstructed weekly malaria cases in 2023 (37 regions)
- Fig. S8 - CwDMD analysis before 5-Year Plan: Decay Mode, phase, and ridgelines (2018)
- Fig. S9 - CwDMD analysis after 5-Year Plan: Oscillatory Mode, phase, and ridgelines (2023)

# Section 1: Analyses for 17 administrative Regions

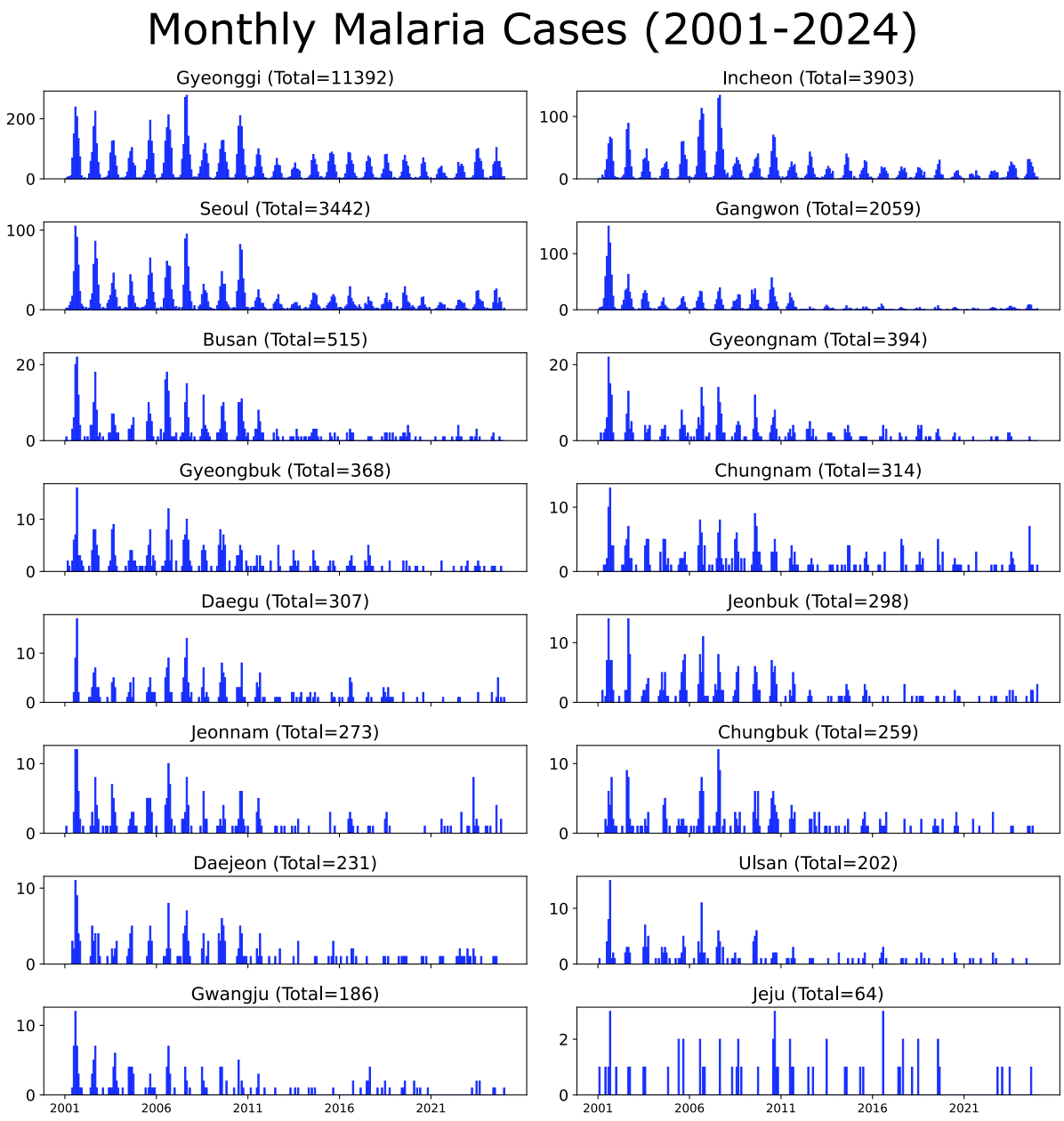


**Fig. S1.** Monthly malaria cases across 17 administrative regions of South Korea from 2001 to 2024. Each panel shows one region, with the total number of reported cases during the study period indicated in parentheses. For consistency, Sejong was aggregated into Chungnam.

**Tab. S1.** Demographic and malaria case statistics in 17 regions of South Korea

| **Region** | **Population (×1,000)** | **Area (km$^2$)** | **Density (per km$^2$)** | **Total cases** | **2007** | **2011** | **2018** | **2023** |
|---|---|---|---|---|---|---|---|---|
| Seoul | 9797.6 | 605.2 | 16189.0 | 3442 | 314 | 93 | 82 | 94 |
| Busan | 3518.6 | 770.2 | 4568.4 | 515 | 41 | 24 | 9 | 7 |
| Daegu | 2444.4 | 883.5 | 2766.7 | 307 | 36 | 16 | 13 | 2 |
| Incheon | 2792.8 | 1065.3 | 2621.6 | 3903 | 484 | 122 | 82 | 126 |
| Gwangju | 1396.1 | 501.2 | 2785.5 | 186 | 7 | 6 | 5 | 5 |
| Daejeon | 1421.2 | 539.6 | 2633.7 | 231 | 23 | 9 | 3 | 6 |
| Ulsan | 1076.8 | 1062.4 | 1013.6 | 202 | 16 | 7 | 4 | 1 |
| Sejong | 390.7 | 465.3 | 839.6 | 8 | 0 | 0 | 1 | 0 |
| Gyeonggi | 11619.6 | 10193.9 | 1139.9 | 11392 | 1007 | 382 | 325 | 434 |
| Gangwon | 1535.1 | 16833.3 | 91.2 | 2059 | 125 | 93 | 11 | 29 |
| Chungbuk | 1543.8 | 7418.2 | 208.1 | 259 | 30 | 11 | 3 | 2 |
| Chungnam | 2027.4 | 8254.7 | 245.6 | 314 | 23 | 12 | 8 | 8 |
| Jeonbuk | 1872.6 | 8072.1 | 232.0 | 298 | 23 | 12 | 5 | 6 |
| Jeonnam | 1944.1 | 12335.7 | 157.6 | 273 | 20 | 11 | 6 | 14 |
| Gyeongbuk | 2658.0 | 18964.3 | 140.2 | 368 | 35 | 11 | 3 | 6 |
| Gyeongnam | 3167.4 | 10534.6 | 300.7 | 394 | 41 | 13 | 13 | 5 |
| Jeju | 608.6 | 1850.8 | 328.8 | 64 | 2 | 4 | 3 | 2 |

Table presents demographic and geographic attributes (population in thousands, area in km$^2$, density per km$^2$), total cumulative malaria cases, and annual cases in selected years (2007, 2011, 2018, 2023). Sejong data are reported separately but often combined with Chungnam in other datasets.

# Section 2: Analyses for 37 Subdivided Regions

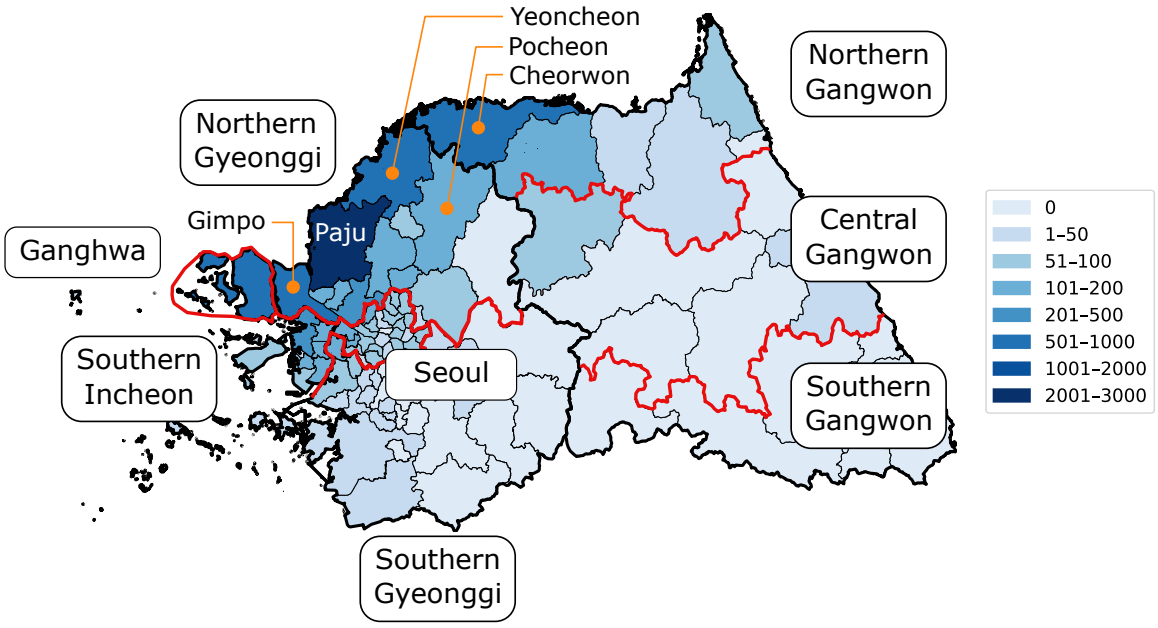


**Fig. S2.** Regional distribution of malaria cases in South Korea and subdivision of high-risk provinces. The map shows cumulative malaria incidence by subregion, with darker shading indicating higher case counts. For finer-scale analysis, Incheon was divided into Ganghwa and Southern Incheon; Gangwon into Northern, Central, and Southern Gangwon; and Gyeonggi into Northern and Southern Gyeonggi. Key hotspots such as Paju, Gimpo, Yeoncheon, and Pocheon are highlighted. In total, these subdivisions yielded 37 distinct regions used in the subsequent analysis. These subdivisions were adopted for the CwDMD-based spatiotemporal analysis.

**Tab. S2.** Regional total malaria cases for the target years

| Region | 2007 | 2011 | 2018 | 2023 | Region | 2007 | 2011 | 2018 | 2023 |
|---|---|---|---|---|---|---|---|---|---|
| Seoul | 301 | 84 | 74 | 90 | Osan | 4 | 0 | 0 | 1 |
| Ganghwa | 219 | 51 | 13 | 20 | Yongin | 10 | 9 | 2 | 4 |
| Gapyeong | 3 | 1 | 1 | 1 | Uiwang | 4 | 2 | 1 | 1 |
| Goyang | 121 | 50 | 57 | 58 | Uijeongbu | 15 | 9 | 7 | 3 |
| Gwacheon | 1 | 2 | 0 | 0 | Icheon | 3 | 0 | 2 | 2 |
| Gwangmyeong | 10 | 2 | 5 | 8 | Paju | 247 | 96 | 66 | 151 |
| Gwangju | 5 | 1 | 6 | 2 | Pyeongtaek | 3 | 2 | 2 | 2 |
| Guri | 3 | 3 | 1 | 0 | Pocheon | 14 | 22 | 10 | 3 |
| Gunpo | 11 | 0 | 1 | 2 | Hanam | 9 | 0 | 3 | 1 |
| Gimpo | 159 | 23 | 30 | 81 | Hwaseong | 6 | 2 | 3 | 3 |
| Namyangju | 20 | 8 | 8 | 7 | Incheon South | 249 | 62 | 62 | 101 |
| Dongducheon | 8 | 6 | 4 | 1 | Gangwon North | 98 | 83 | 7 | 21 |
| Bucheon | 26 | 7 | 9 | 14 | Gangwon Central | 17 | 7 | 2 | 3 |
| Seongnam | 24 | 4 | 18 | 2 | Gangwon South | 10 | 1 | 1 | 1 |
| Suwon | 17 | 6 | 7 | 7 | Yeoncheon | 151 | 68 | 8 | 25 |
| Siheung | 10 | 7 | 6 | 6 | Yeoju | 0 | 0 | 1 | 0 |
| Ansan | 25 | 8 | 2 | 6 | Yangju | 19 | 7 | 33 | 17 |
| Anseong | 4 | 0 | 2 | 1 | Yangpyeong | 1 | 1 | 2 | 1 |
| Anyang | 12 | 3 | 5 | 3 | | | | | |

Regional total malaria cases during the 29-week active transmission period (April–October) for the target years 2007, 2011, 2018, and 2023 across 37 regions. Values represent the total number of malaria cases aggregated over 29 epidemiological weeks for each region.

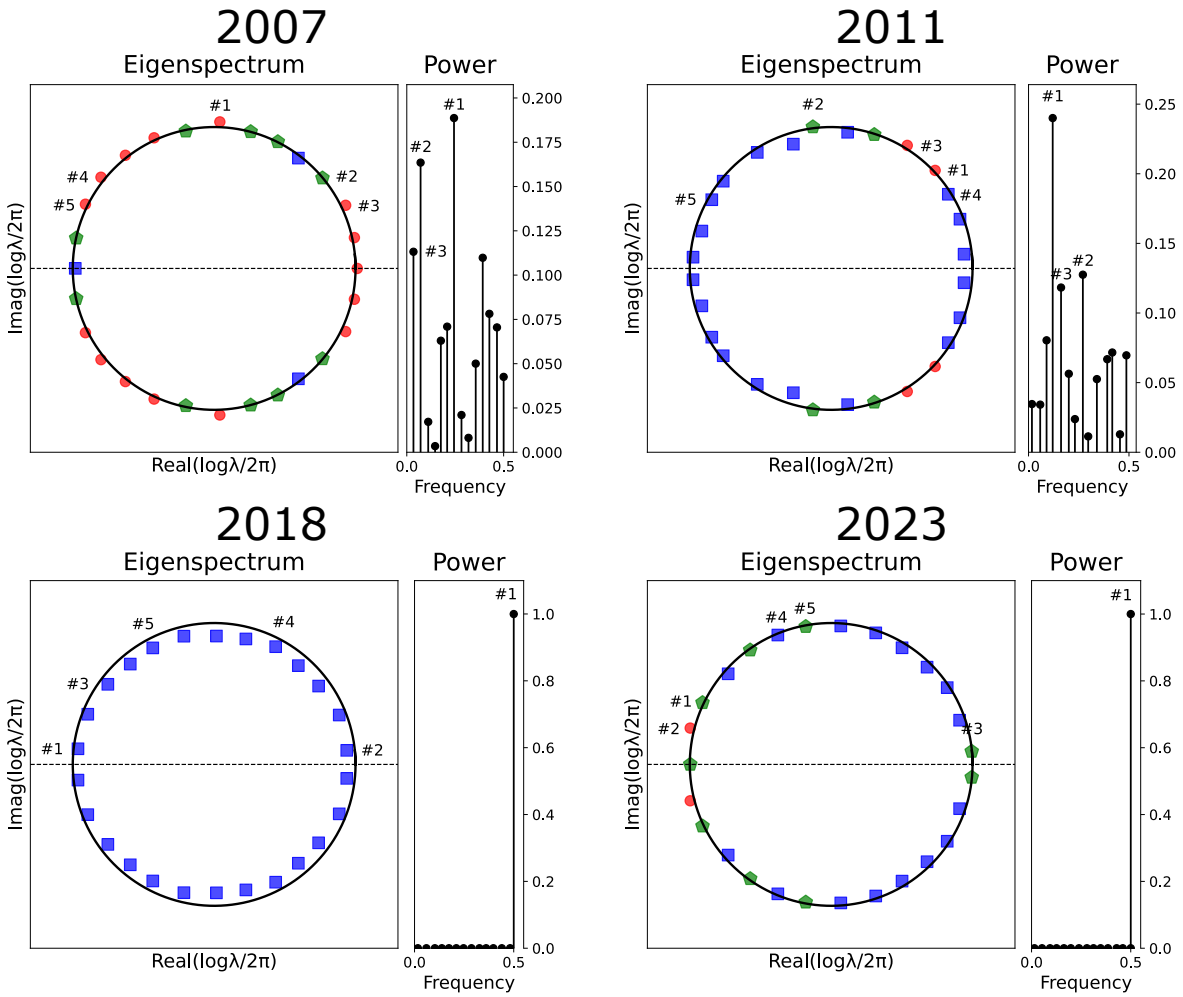


**Fig. S3.** Eigenvalue spectrum of the CwDMD analysis for the target years 2007, 2011, 2018, and 2023. Eigenvalues are plotted in the complex plane relative to the unit circle. Each analysis was performed at a spatiotemporal resolution of $37 \times 29$. Modes are classified by their positions: Growth modes lie outside the unit circle ($|\lambda| > 1$), Decay modes lie inside ($|\lambda| < 1$), and Oscillatory modes lie on or near the unit circle with a nonzero imaginary part. Red circles represent Growth Modes, green pentagons denote Oscillatory Modes, and blue squares indicate Decay Modes. The most dominant mode was identified as a Growth Mode in 2007 and 2011, a Decay Mode in 2018, and an Oscillatory Mode in 2023.

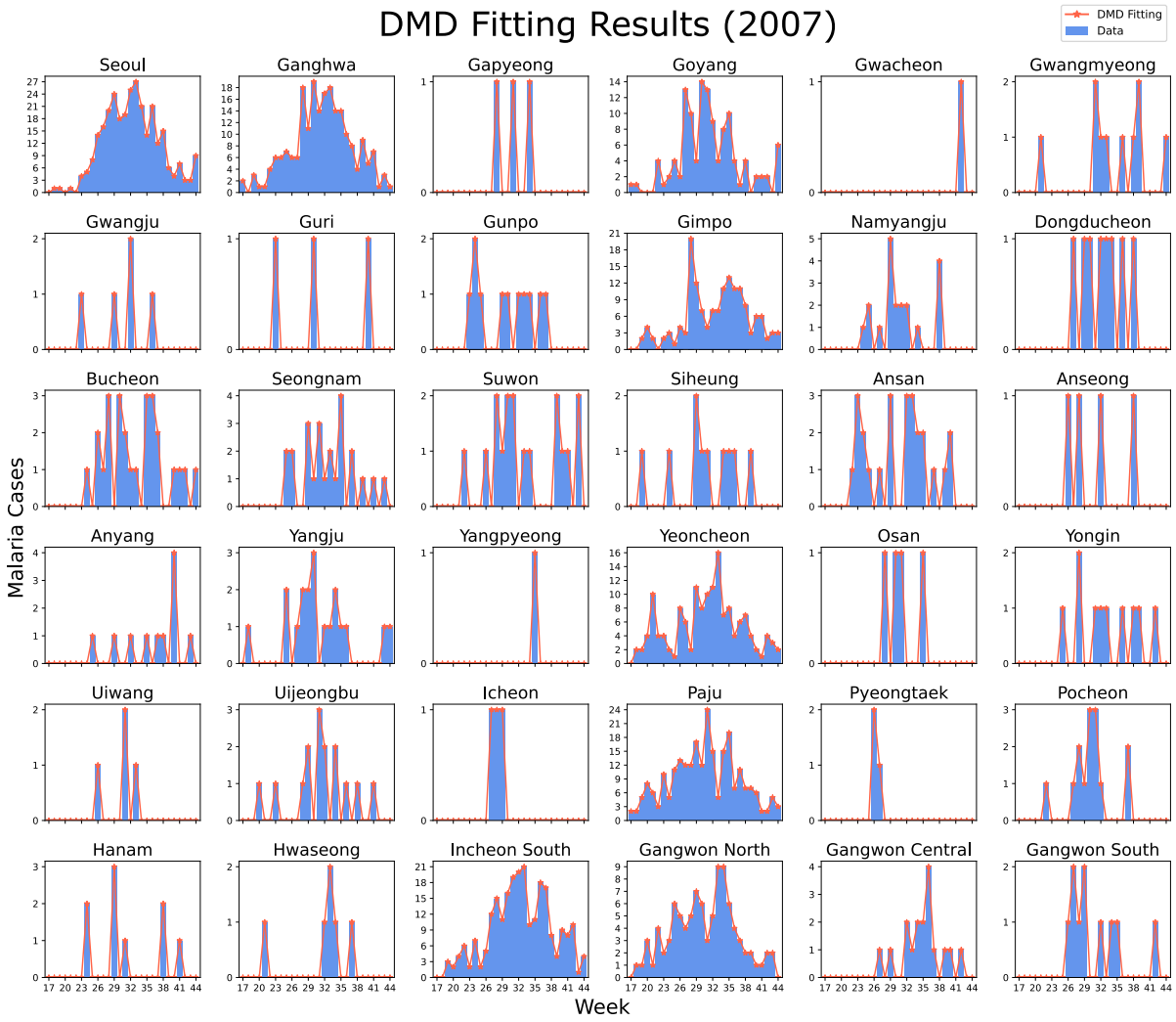


**Fig. S4.** Comparison of observed weekly malaria cases and reconstructed values from the CwDMD analysis across 37 regions in South Korea in 2007 (Yeoju excluded due to zero reported cases). Blue bars represent observed malaria cases, and red lines denote reconstructed values derived from the CwDMD model. The reconstructed results closely reproduce the seasonal fluctuations and magnitudes of the observed data in most regions, validating the accuracy of the CwDMD fitting and confirming the reliability of subsequent phase and magnitude analyses.

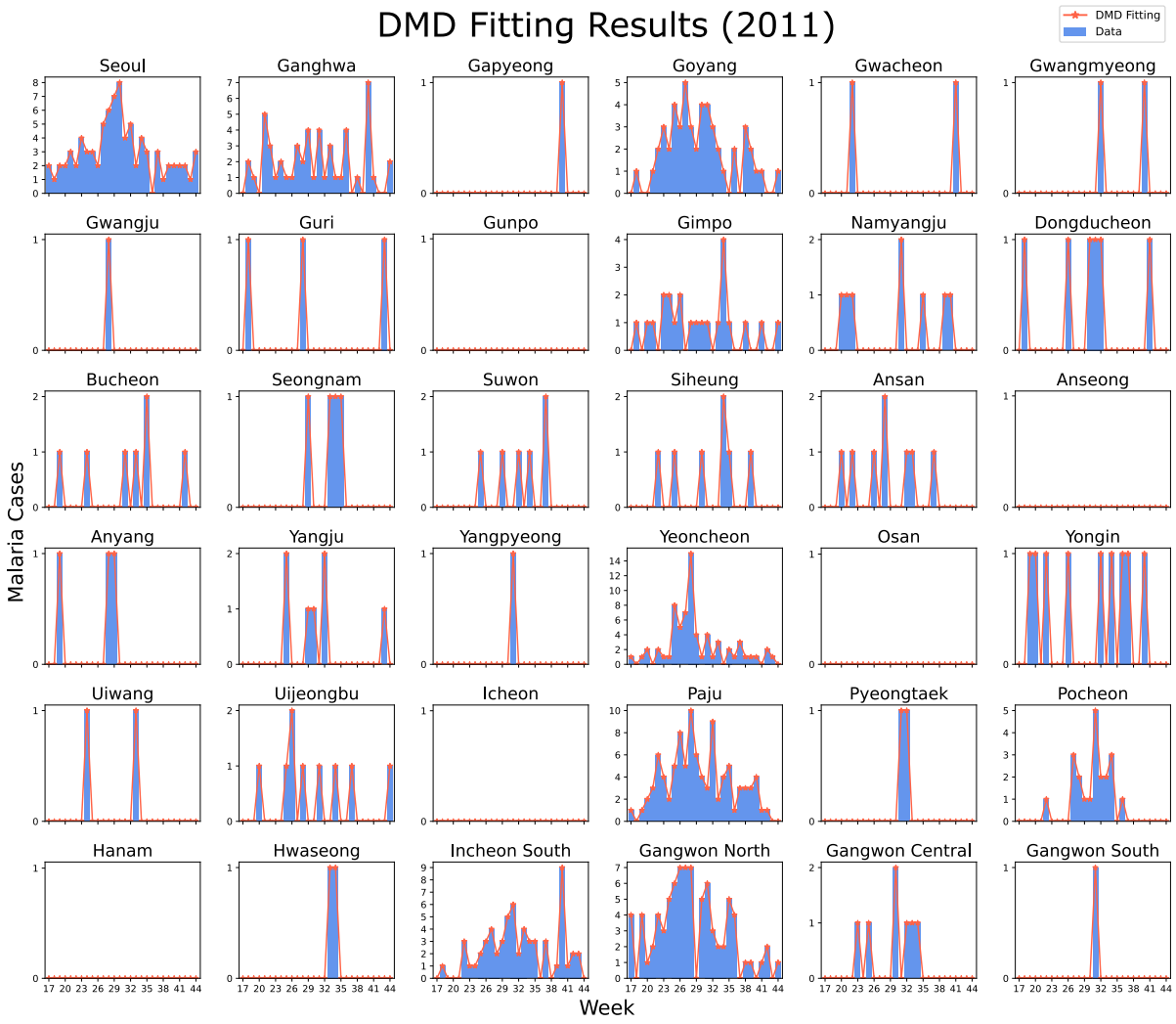


**Fig. S5.** Comparison of observed weekly malaria cases and reconstructed values from the CwDMD analysis across 37 regions in South Korea in 2011 (Yeoju excluded due to zero reported cases). Blue bars represent observed malaria cases, and red lines denote reconstructed values obtained from the CwDMD model. The reconstructed results closely match the seasonal variations and magnitudes of the observed data in most regions, validating the accuracy of the model fitting and supporting the reliability of subsequent analyses.

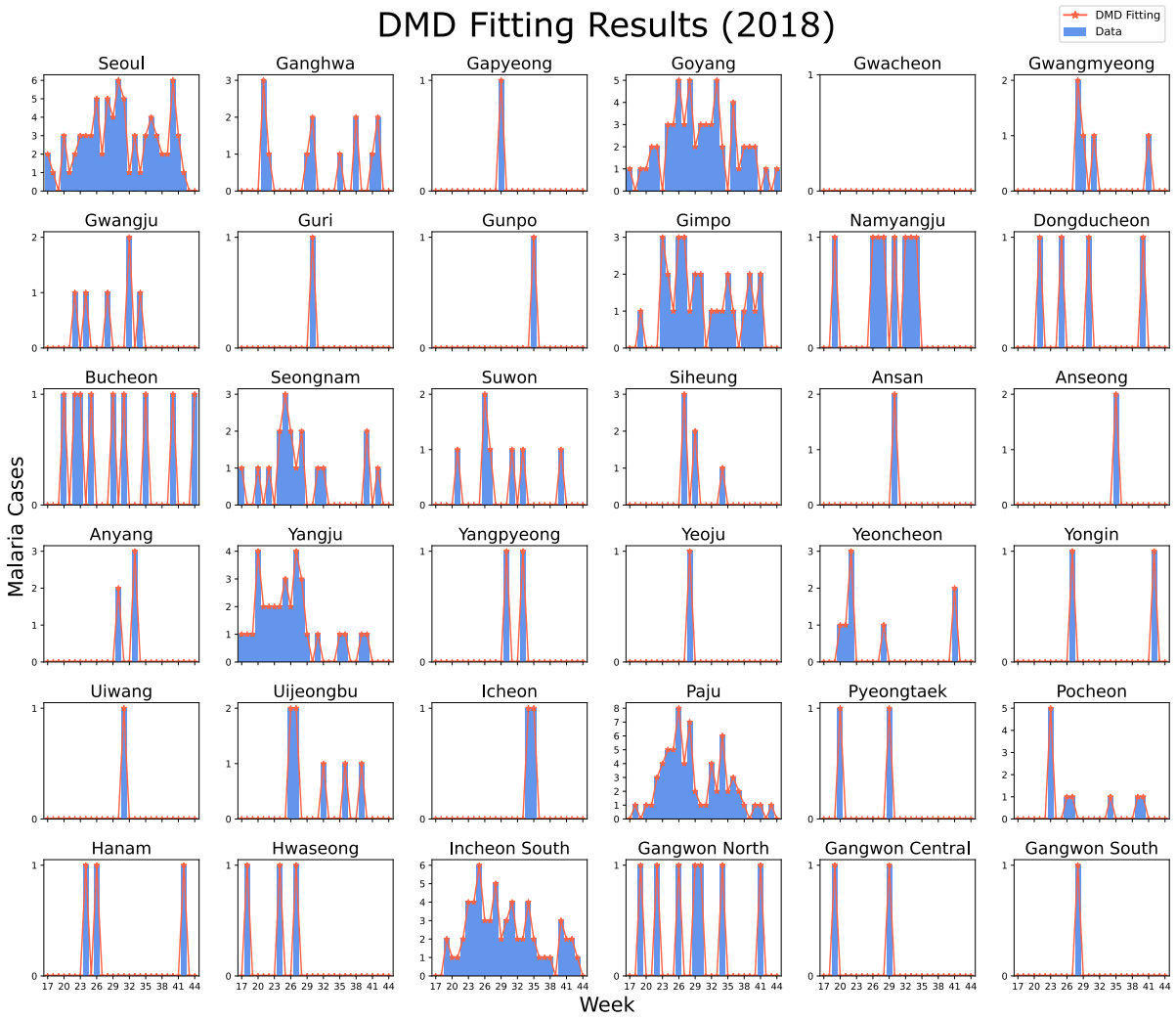


**Fig. S6.** Comparison of observed and reconstructed weekly malaria cases across 37 regions in South Korea in 2018 (Osan excluded due to zero reported cases). Blue bars represent observations, and red lines denote reconstructed values derived from the CwDMD model. The reconstructed results accurately reproduce the observed seasonal peaks and amplitudes in most regions, validating the consistency of the CwDMD fitting and confirming its robustness for spatiotemporal analysis.


**Fig. S7.** Comparison of observed and reconstructed weekly malaria cases across 37 regions in South Korea in 2023 (Yeoju excluded due to zero reported cases). Blue bars represent observed data, and red lines denote reconstructed values derived from the CwDMD analysis. The reconstructed results closely match the observed seasonal patterns across most regions, confirming the reliability of the CwDMD fitting for all target years.

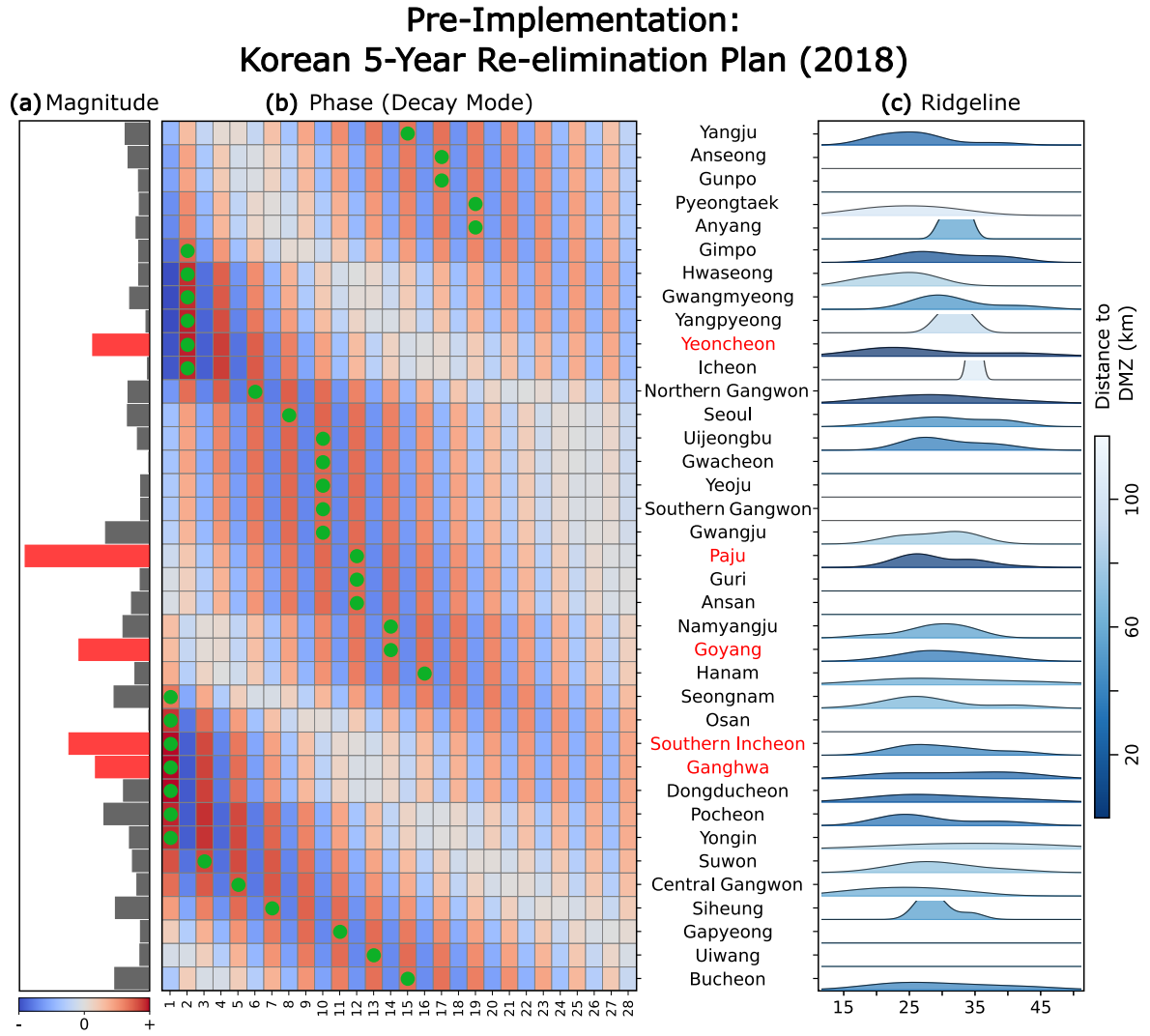


**Fig. S8.** CwDMD analysis of malaria transmission dynamics in 2018, prior to the implementation of the Korean 5-Year Malaria Re-Elimination Plan. (a) Magnitude distribution of the dominant Decay Mode (37 regions × 29 weeks), indicating the strength of the mode in each region. (b) Phase structure of the same mode (reference = Paju); color encodes the regional peak offset (weeks) relative to Paju, centered at 0 (same week), with blue indicating earlier peaks and red indicating later peaks. Green circles mark the peak week for each region and were slightly adjusted along the temporal axis to provide smoother alignment for clearer comparison of inter-regional phase differences, without altering the original phase trajectories. (c) Ridgeline plots of weekly malaria case densities by region; curves are colored by each region's mean distance from the DMZ (km). The five regions with the highest magnitudes are highlighted in red. Together, the panels illustrate weakened temporal synchronization across regions and a gradual disintegration of inter-regional connectivity prior to the policy implementation.

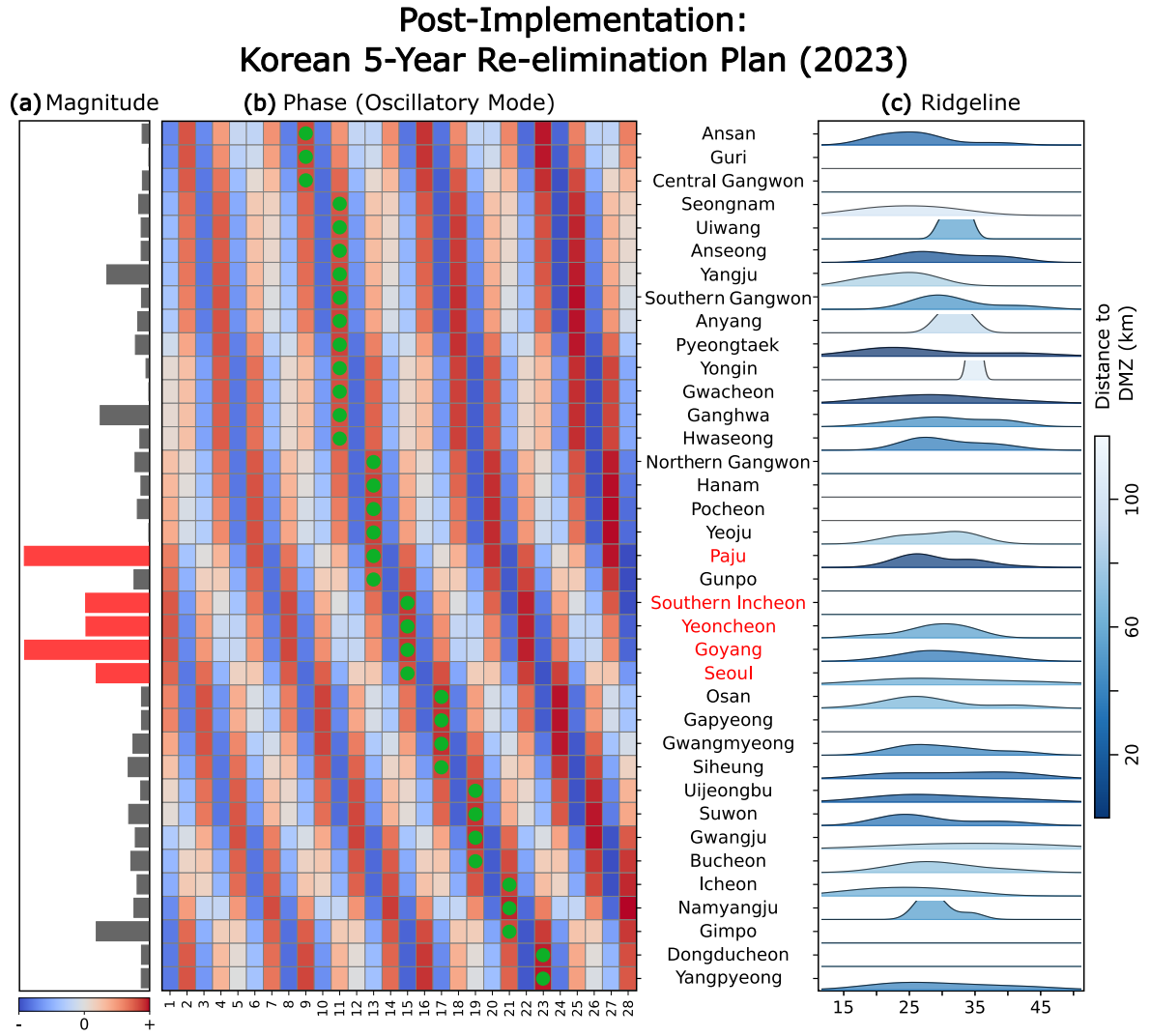


**Fig. S9.** CwDMD analysis of malaria transmission dynamics in 2023, following the implementation of the Korean 5-Year Malaria Re-Elimination Plan. (a) Magnitude distribution of the dominant Oscillatory Mode (37 regions × 29 weeks), indicating the strength of the mode in each region. (b) Phase structure of the same mode (reference = Paju); color encodes the regional peak offset (weeks) relative to Paju, centered at 0 (same week), with blue indicating earlier peaks and red indicating later peaks. Green circles mark the peak week for each region and were slightly adjusted along the temporal axis to provide smoother alignment for clearer comparison of inter-regional phase differences, without altering the original phase trajectories. (c) Ridgeline plots of weekly malaria case densities by region; curves are colored by each region's mean distance from the DMZ (km). The five regions with the highest magnitudes are highlighted in red. Together, the panels show reinforced synchronization among high-risk regions in 2023, consistent with the resurgence of malaria transmission after the policy period.